Effects of Sudden Commencement on the Ionosphere: PFISR Observations and Global MHD Simulation

Shasha Zou[1], Dogacan Ozturk[1], Roger Varney[2], Ashton Reimer[2]

1. Department of Climate and Space Sciences and Engineering, University of Michigan, MI, USA
2. Center for Geospace Studies, SRI International, Menlo Park, CA, USA

Abstract:

Sudden commencement (SC) induced by solar wind pressure enhancement can produce significant global impact on the coupled magnetosphere-ionosphere (MI) system, and its effects have been studied extensively using ground magnetometers and coherent scatter radars. However, very limited observations have been reported about the effects of SC on the ionospheric plasma. Here we report detailed Poker Flat incoherent scatter radar (PFISR) observations of the ionospheric response to SC during the March 17, 2015 storm. PFISR observed lifting of the F-region ionosphere, transient field-aligned ion upflow, prompt but short-lived ion temperature increase, subsequent F-region density decrease, and persistent electron temperature increase. A global Magnetohydrodynamic (MHD) simulation has been carried out to characterize the SC-induced current, convection and magnetic perturbations. Simulated magnetic perturbations at Poker Flat

This is the author manuscript accepted for publication and has undergone full peer review but has not been through the copyediting, typesetting, pagination and proofreading process, which may lead to differences between this version and the Version of Record. Please cite this article as doi: 10.1002/2017GL072678

show a satisfactory agreement with observations. The simulation provides a global context for linking localized PFISR observations to large-scale dynamic processes in the MI system.

Key points:

1. PFISR observed ionospheric plasma responses to field-aligned currents and ionospheric convection vortices formed during sudden commencement.
2. Ionosphere responses include F-region plasma lifting, field-aligned ion upflow, density decrease, short-lived T_i increase and long lasting T_e increase.
3. Global MHD simulation reproduced the magnetic perturbation on the ground and revealed SC-related FACs and convection evolutions.

1. Introduction

A sudden increase of solar wind dynamic pressure associated with an interplanetary shock or a discontinuity leads to a large-scale compression of the magnetosphere, and such a compression is referred to as sudden commencement (SC) based on the ground-based magnetometer observations. SC is usually used to describe a broad range of phenomena, including sudden storm commencement (SSC) and sudden impulse (SI) [see review by *Curto et al.*, [2007] and references therein], and emphasizes the compression effect associated with dynamic pressure enhancement regardless of whether or not a geomagnetic storm follows the compression. The effects of sudden commencement on the coupled magnetosphere-ionosphere system have been studied extensively by using ground-based magnetometers and SuperDARN coherent radars [e.g., *Nishida and Jacobs*, 1962; *Araki*, 1977, 1994; *Kikuchi et al., 2001*; *Shi et al.*, 2014; *Tian et al.*, 2016]. Depending on the polarities of the magnetic field perturbation and the field-aligned currents (FACs), the response of the coupled system can be characterized into two phases, i.e., the preliminary impulse (PI) phase and the main impulse (MI) phase [*Araki*, 1994]. In general, during the PI phase, the field-aligned currents (FACs) are downward/upward in the afternoon/morning sector and the associated Hall currents inferred from ground-based magnetometers form a counterclockwise/clockwise vortex. During the MI phase, the polarities of the FACs, the direction of the Hall currents and the convection flows reverse.

The formation mechanisms of the PI and MI phases caused by the solar wind dynamic pressure enhancement have been investigated through theoretical studies [e.g. *Kivelson and Southwood*, 1991; *Araki*, 1994] and numerical modeling, mainly global magnetohydrodynamic (MHD) simulations [e.g. *Slinker et al.*, 1999; *Fujita et al.*, 2003a, 2003b, 2005; *Chi et al.*, 2006; *Samsonov et al.*, 2010; *Yu and Ridley*, 2011; *Sun et al.*, 2015; *Kubota et al.*, 2015; *Tian et al.*, 2016]. In these studies, the solar wind dynamic pressure front has been assumed to be of large scale and approach the magnetosphere as a planar discontinuity. Smaller scale magnetic disturbances sometimes occur on the dayside high-latitude magnetosphere, and they are often called magnetic impulse event [*Lanzerotti et al.*, 1991; *Sibeck and Korotova*, 1996], which are associated with smaller scale ionospheric convection vortices (traveling convection vortices, or TCVs) and FACs systems [*Friis-Christensen et al.*, 1988; *Glassmeier et al.*, 1989]. These smaller-scale features are suggested to arise from localized solar wind dynamic pressure enhancement or dynamic processes in the foreshock region [e.g., *Moretto et al.*, 1997; *Zesta et al.*, 1999, 2002; *Murr et al.*, 2002; *Sibeck et al.*, 2003; *Murr and Hughes*, 2003; *Kataoka et al.*, 2003]. *Kataoka et al.* [2003] simulated the FACs systems associated with TCVs by introducing a localized density perturbation and found that the FACs produced have the same polarities as those induced by large-scale solar wind dynamic pressure enhancement but with much smaller scale sizes.

Despite numerous studies on the effects of SC on the coupled geospace system, there have been only very limited studies on the effects of SC and the associated transient FACs and convection flows on the ionospheric plasma. *Doupnik et al.* [1977] used Chatanika incoherent scatter radar (ISR) and magnetometers in Alaska to study the ionosphere response to three SCs within one day and founded that enhanced ionospheric convection flows occurred during two of the three SC events. Using the EISCAT radar and magnetometers, *Collis and Häggström* [1991] performed a case study of the ionospheric plasma response to SC. They observed F-region electron density depletion, ion temperature increase and increased horizontal convection flow, but no field-aligned ion upflow event was observed in their case study. These two pioneer works showed the possible effects of SC on ionospheric plasma, but could not connect the localized ISR observations with either solar wind measurements or large-scale magnetospheric drivers. *Schunk et al.* [1994] modeled the ionospheric response to a pair of FACs and ionospheric vortices with spatial scales similar to TCVs using the Utah State University time-dependent ionospheric model. Their simulation results revealed localized plasma temperature enhancements, in particular ion temperature, ion composition changes, non-Maxwellian ion distributions, and plasma upwelling.

The terrestrial ionosphere supplies plasma to the magnetosphere through the ion outflow

process, in particular the heavy ions such as O^+. The O^+ ions play an important role in regulating the dynamics in the magnetosphere, such as changing the ion composition in the ring current and thus its life time, affecting the reconnection rate both at the dayside magnetopause and in the nightside magnetotail [e.g., *Chappell,* 2015; *Lotko,* 2007 and references therein; *Yau,* 2007 and references therein]. *Strangeway et al.* [2005] suggested that ion outflow usually occurs as a two-step process with ion upflow caused by increased ion (so-called Type 1 upflow) and/or increased electron (so-called Type 2 upflow) temperatures in the F-region and topside ionosphere as the first step. Recently, enhanced F-region and topside ionosphere density within the storm-enhanced density (SED) region [*Foster et al.,* 2005; *Zou et al.,* 2013, 2014] has been suggested to be a third mechanism of contributing large ion upflow fluxes [*Semeter et al.,* 2004; *Yuan et al.,* 2008; *Zou et al.,* 2017]. The first two mechanisms described above arise from plasma temperature increase, while the third one associated with SED is due to increased plasma source population. Ion upflow pumps the ionospheric plasmas to higher altitudes where they can be further accelerated to velocities exceeding the escape velocity. It has also been suggested that the initial ion upflow flux in the F region and topside ionosphere can regulate the total flux of ion outflow [*Nilsson et al.,* 2008]. Therefore, understanding the generation mechanisms of the initial ion upflow under various interplanetary and geomagnetic conditions is of great importance for understanding the ion outflow processes. Statistical studies have shown that the ion upflow fluxes increase with

increasing solar wind density and velocity [*Ogawa et al.*, 2009]. However, there are only very limited studies devoted to identifying the physical processes that generate the ion upflow associated with solar wind pressure enhancement.

Ground-based coherent scatter radar requires field-aligned density irregularities in the F region in order to scatter the radar signals back. There have been a few studies on the effects of the SC on the radar performance [*Kataoka et al.*, 2003; *Kane and Macarevich*, 2010; *Gillies et al.*, 2012]. *Kataoka et al.* [2003] found enhanced F-region irregularities excited due to local and strong F-region density gradient within the convection flow vortex. Using a superposed-epoch analysis, *Gillies et al.*, [2012] found that ionospheric plasma drift and radar echoes both increase on the dayside due to the dynamic pressure increase, while the coherent radar irregularities decrease on the nightside despite that the flow speed continues to increase. Therefore, understanding the response of the ionospheric plasma to solar wind dynamic pressure enhancement can help improve the understanding of the related field-aligned irregularities and advance the forecast capability of coherent radar coverage.

Instrument limitation is part of the reason why the ionospheric response to solar wind dynamic pressure enhancement has not been studied extensively. Multi-parameter vertical profiles of the ionospheric plasma can only be provided by ground-based ISR.

Traditional ISRs need to mechanically shift the antenna steering direction, thus the temporal resolution for covering multiple directions is limited. In recent years, the advanced modular incoherent scatter radar (AMISR) [*Heinselman and Nicolls*, 2008] utilizes phased array technique and enables high-resolution and multi-directional observations of the ionosphere, which are particularly useful for studying the ionosphere response to transient solar wind perturbations, such as dynamic pressure increase.

In this study, we present a detailed case study of the ionospheric response to the solar wind dynamic pressure enhancement associated with the March 17, 2015 geomagnetic storm sudden commencement (SSC), and the resulting FACs and ionospheric convection flows by using data from Poker Flat incoherent scatter radar (PFISR) and ground-based magnetometers. We have also carried out a global MHD simulation of the coupled magnetosphere-ionosphere for this storm event to obtain a global context for interpreting localized ISR observations. Results from the global MHD simulation and their comparisons with ground-based measurements will be presented.

2. Observations and Modeling

2.1. Solar wind and IMF observations

The March 17, 2015 storm with the minimum Sym-H reaching -234 nT was caused by an interplanetary coronal mass ejection (ICME) and has received much attention. The SSC

at ~0445 UT on March 17, 2015 was initiated by the shock formed in front of the ICME. Figure 1 shows the solar wind and IMF conditions propagated to the bow shock from the OMNI database. The solar wind velocity elevated from ~400 to ~500 km/s, while the solar wind proton number density increased from ~10 to ~35 cm^{-3}. As a result, the dynamic pressure jumped from ~5 to ~18 nPa. The IMF Bz turned further northward from ~10 nT to ~25 nT and lasted for more than an hour before rotated into a southward direction. In this study, we focus on the response of the ionosphere to this solar wind dynamic pressure enhancement. The bottom panel of Figure 1 shows the 1-min Sym-H index, from which the compressional effect of the SSC can be seen clearly at ~0445 UT.

2.2. Magnetometer and PFISR observations

Figure 2a shows the 1-sec H-component perturbation measured by the Poker Flat ground-based magnetometer from 0430 UT to 0530 UT on March 17, 2015. The perturbation shown in this panel is obtained by subtracting a baseline value, which is taken as the mean value between 0430 and 0440 UT. The perturbation shows a clear negative perturbation, i.e., the preliminary impulse (PI), at ~0445 UT followed by a positive perturbation, i.e., the main impulse (MI), which lasted much longer. This magnetic perturbation is consistent with the classic magnetic signatures of SC.

PFISR was running in the four-beam international polar year (IPY) mode before 0500 UT on March 17, 2015. There was one beam pointing in the direction parallel to the magnetic

field (beam 2, UpB), one beam pointing vertically (beam 1), and two other beams pointing to higher latitudes with lower elevation angles (beams 3 and 4). At the time of the storm SSC, PFISR was located at ~17.7 MLT on the dusk side and its observations from 0430 to 0500 UT are shown in Figure 2b-2d. The first three panels (2b-2d) show the convection flow direction, magnitude, and vector as a function of UT and magnetic latitude (mlat), respectively. Calculations of the ExB convection flow and the antiparallel flow from AMISR data can be found in *Heinselman and Nicolls*, [2008]. In the Northern hemisphere, the antiparallel direction is positive pointing to higher altitudes along the magnetic field. Given a ~78° magnetic field inclination at PFISR, both the ExB convection flow and the antiparallel flow can provide finite vertical flows, either positive or negative, when projected to the geographic vertical direction [*Zou et al.,* 2013, 2014]. A schematic illustration of the flow geometry is provided on the right of Figure 2f. Figure 2e shows the total plasma vertical flows calculated by combining the contributions from the ExB convection flow and the antiparallel flow in the vertical direction. The latitudinally averaged vertical flows contributed by the ExB convection flow (red) and the antiparallel flow (blue) are illustrated in Figure 2f. The bottom panel (2g) shows the altitude profiles of electron density measured by the vertical beam, i.e., beam 1. As one can see, in general, before the SSC, the convection flows at PFISR were very weak and the F-region ionosphere resembled the quiet time conditions. After the SSC, there were large convection flow perturbations, F-region plasma lifting to higher altitudes and

subsequent decrease of the F-region plasma density. As shown in Figures 2e-2f, strong plasma vertical flows lasted about 4 minutes starting at the transition time from the PI to the MI phase at ~0447 UT, and the flow speed reached > 200 m/s almost purely due to the contribution from the ExB convection flows. Such vertical drift and lifting of the F-region ionosphere have been frequently observed within the SED [*Zou et al.,* 2013, 2014] although the convection flows are associated with different magnetospheric dynamic processes. These vertical drifts and F-region lifting have been suggested to play an important role in preconditioning intense ion upflow fluxes [*Zou et al.,* 2017].

Figure 3 shows the altitude profiles of (a) electron density N_e, (b) line-of-sight velocity V_{los}, (c) ion temperature T_i, and (d) electron temperature T_e from the 5-min integrated long pulse measurement of the vertical beam. The 5-min integrated long pulse data are chosen to show because they have better signal-to-noise ratio (SNR) and thus are less noisy, while the 1-min integrated long pulse data have also been studied. Grey curves show the measurements obtained during the three integration time (~ 15 min) prior to the SSC, while colored curves show the values during the SSC and afterwards. The integration time corresponding to each color curve is also denoted. The density profiles in Figure 3a indicate that the height of the F-region peak density (h_mF_2) rose from ~290 km to ~330 km, resulting in a 40 km increase. At the same time, the peak density (N_mF_2) decreased from ~$7x10^{11}$ to 4.5 $x10^{11}$ m^{-3}, a 36% decrease. The total electron content

(TEC) calculated by integrating the density along the altitude up to the topside ionosphere (~650 km) shows a > 7 TECU (1 TECU = 10^{16} electrons/m^2) reduction when comparing the averaged TEC between 0435-0440 UT, i.e, 5-10 min before the compression and that between 0455-0500 UT, i.e., 10-15 min after the compression.

Figure 3b shows that the vertical flow velocity was, in general, around zero despite large measurement uncertainties, but the flow velocity above 250 km altitude was clearly upward immediately after the SSC, consistent with the lifting signatures in Figure 2e-f and the electron density in Figure 2g. In Figure 3c, T_i increased from ~1000 K to more than 2000 K at all altitudes above ~ 150 km immediately after the SSC (blue curve), but dropped back to quiet time values in the subsequent measurements ~ 5 min later (green and red curves). The T_i increase was particularly large below ~200 km albeit with relatively large uncertainties because of the low electron density in this region. In contrast, T_e shown in Figure 3d increased from below 1500 K to above 2000 K above 200 km and lasted for at least three integration time (~15 min) until ~0500 UT, i.e., the end of this experiment.

A field-aligned ion upflow/downflow event is defined when three consecutive field-aligned velocity data are larger/smaller than 100/-100 m/s [*Ogawa et al.*, 2009]. According to this criterion, we did not find any field-aligned ion upflow events in the

UpB beam (beam 2) in the 5-min integrated long pulse data. We, therefore, turned to the 1-min integrated long pulse data of the UpB beam to examine whether there are signatures of field-aligned ion upflow. Figure 3e shows the 1-min field-aligned line-of-sight velocity measured by beam 2 from 0447:22 UT to 0449:42 UT (i.e., ~2 min interval). Because of short integration time, the data become very noisy. Only data points with measurement uncertainties smaller than the magnitude of measurement itself are plotted here. Two dashed vertical lines at 0 m/s and 100 m/s are plotted to help identify the upflow event. The averaged field-aligned ion upflow velocity from range gate 7 to range gate 11 (i.e., from 274 km to 392 km) during 0447:22-0448:32 UT (red) reached ~190.7 m/s, while that from range gate 6 to range gate 8 (i.e., from 250 km to 321 km) at 0448:32-0449:42 UT (blue) reached ~133.5 m/s. *Collis and Häggström* [1991] commented that they did not find field-aligned ion upflow during the SC event they studied. To the best of our knowledge, this transient field-aligned ion upflow due to SC have not been reported before.

The T_i increase occurred at the same time as the SC-related convection flow speed increase , and therefore, this increase is likely due to enhanced frictional heating. Similar but persistent T_i and V_{los} increases due to frictional heating have also been observed during the main phase of the same storm but in the subauroral polarization stream (SAPS) region by the Millstone Hill radar [*Zhang et al.*, 2017]. Significant and persistent

frictional heating can also increase the neutral temperature and lead to neutral upwelling, as found in the SAPS region by *Zhang et al.,* [2017]. However, because the neutrals need much longer time (tens of minutes to days) to respond to frictional heating [*Schunk and Nagy,* 2009], it is unlikely to have such neutral upwelling formed within the first 5-10 minutes right after the onset of the strong horizontal flows due to the SC.

The cause of the long-lasting T_e increase appears more complicated, and could be due to a combined effect of electron density reduction and potential particle precipitations associated with upward FACs related to the SC. Assuming no extra incoming energy, the electron temperature and the density should be anti-correlated with each other [*Schunk and Nagy,* 2009]. So if the electron density decreases, its temperature can increase. The observed plasma temperature changes and their temporal variations are consistent with the simulation results reported in *Schunk et al.* [1994], who showed short-lived T_i enhancement at the front of vortices and long lasting T_e effect in the wake of vortices.

The blue curve in Figure 3c shows that T_i was larger than T_e and there was a temperature bulge in the T_i profile near ~200 km. This could be a signature of enhanced frictional heating, but the retrieval of T_i in ISR fitting is also subject to uncertainties with the assumption of stationarity and with the assumed molecular ions concentrations [*Zettergren et al.* 2011]. Rapidly varying line-of-sight velocities over the integration

period can broaden the integrated spectrum, leading to an overestimation of ion temperature after fitting, but in this case this effect is not expected to be significant because the high temperatures are still observed when the data is reprocessed with a 1-minute integration time. Intense frictional heating events will also increase the fractional concentration of NO^+ since the $O^+ + N_2 \rightarrow NO^+ + N$ reaction is highly temperature dependent [*Schunk and Nagy,* 2009]. The standard PFISR data fitting procedure uses the FLIP chemistry model developed by *Richards and Voglozin* [2011], so the effect of the chemical composition change has been considered here to within the limits of validity of that model. After the convection flow enhancements and plasma temperature increases, the concentrations of molecular ions NO^+ and O_2^+ increased to ~84% and ~12% at the range gate of 197 km, respectively, and the O^+ concentration decreased to ~3%. In addition, we have also explored the sensitivity of the estimated T_i by investigating an ensemble of composition profiles and assuming the original fitter correctly estimated the density weighted average T_i/m_i (see supporting information S1). While the T_i temperature bulge becomes less prominent when the transition height is lower, it still exists even with the lowest transition height tested. This experiment suggests that the temperature bulge in the T_i altitude profile observed near 200 km is likely due to very strong frictional heating, and not purely due to the ion composition changes.

As shown in *Schunk et al.* [1994], the perpendicular ion temperature is expected to be much higher than the parallel temperature. PFISR observations show less T_i enhancement

in the UpB beam and more T_i enhancement in the two lower-elevation beams, as expected if $T_{perp} > T_{parallel}$. However, we have attempted to derive the temperature anisotropy by using different combinations of the 4 beams and assuming spatial uniformity, and our analysis yielded different results, implying that the temperature enhancements are not spatially uniform between the beams. Accurate determination of the temperature anisotropy would require improved measurement techniques, such as multiple ISRs [e.g. *Ogawa et al.,* 2000] or bi-static measurements. In addition, non-maxwellian ion distribution functions in the perpendicular plane can lead to systematic overestimation of ion temperature when observed at large aspect angles and underestimation of ion temperature when observed at small aspect angles [*Wisner et al.,* 1989]. None of the ISR spectra in any of the beams show the formation of a central peak associated with non-maxwellian ion distribution functions; however, all of the beams in this experiment have small aspect angles (<15°) and are not expected to be sensitive to non-maxwellian distribution function signatures. The properties of the perpendicular ion distribution function cannot be determined from the beam geometry in this experiment.

2.3. Global MHD simulation

To investigate the ground magnetic field perturbations associated with the TCVs due to solar wind pressure enhancement, their propagation and the associated currents, we have performed a global MHD simulation by using the coupled BATSRUS [*Tóth et al.*, 2012],

Ridley ionosphere electrodynamic module [*Ridley et al.*, 2004] and CRCM model [*Fok et al.*, 2001; *Buzulukova et al.*, 2010; *Glocer et al.*, 2013]. Solar wind and IMF observations from the WIND spacecraft have been used as upstream conditions to drive the coupled model. Because of the uncertainty of solar wind and IMF propagation from the spacecraft to the upstream boundary of the simulation, the modeled results have been shifted 16 min to match the observed compression time registered in the Sym-H index.

A virtual ground magnetometer [*Yu and Ridley,* 2011] at the location of Poker Flat has been included in the simulation. The simulated H-component perturbations at Poker Flat are shown in Figure 4a (blue), which agrees very well with the observation at Poker Flat (red). The good agreement between the observed and modeled magnetic perturbations provides us confidence in using the global model to study the pressure induced FACs, convection and their evolution and to interpret the PFISR observations presented above.

Besides the virtual magnetometer at Poker Flat, a total of 100 uniformly distributed virtual magnetometers between 50° to 80° mlat and every 2 hours of MLT in the Northern hemisphere have also been included in the simulation and their H-component perturbations are shown as color contours in Figures 5b and 5c at the time of the dip of the PI phase and the peak of the MI phases. The location of Poker Flat is denoted by the cyan dots. Contributions to the H-component perturbation from four different types of

currents, including Hall and Pederson currents, FACs and magnetospheric currents, have been quantified and compared (not shown). We found that the dominant contribution to the total perturbation is the Hall currents, consistent with the *Fukushima* theory [*Fukushima,* 1976].

At 0446 UT, the negative PI phase observed at Poker Flat was part of a cloud of negative perturbation surrounding the dayside (Figure 4b). The FACs superimposed with convection contours on top are shown in Figures 5d and 5e. The FACs plot in Figure 4d shows that around this time, Poker Flat was located close to the boundary between the downward FACs associated with the PI and the upward FACs associated with the MI. Thus the negative perturbation can be understood to be due to the Hall currents flowing northwestward between the two FAC systems.

The FACs continue to propagate with time from the day side to the night side as well as moving poleward. Consequently, the positive H perturbation observed by the Poker Flat magnetometer around 0448UT during the MI phase was part of the positive perturbation cloud (Figure 4c) and was due to the Hall currents flowing southeastward between the MI upward FACs and the weak downward FACs at lower latitudes.

The polarities of FACs can also be inferred from the convection flow measurements from PFISR in Figure 2. The results are consistent with the findings from our global simulation. That is, the closure Hall currents poleward and equatorward of the upward FACs passed PFISR during the PI and MI phases sequentially. The F-region lifting observed in Figure 2 happened mainly due to the poleward and northwestward convection flows during the transition from the PI phase to the MI phase.

3. Summary and Conclusions

SC due to the solar wind dynamic pressure enhancements have been studied extensively using ground magnetometers and SuperDARN radars, while only very limited studies have been reported about the effects of the SC on the ionospheric plasma. Here we report detailed PFISR observations of the ionospheric responses to the solar wind dynamic pressure enhancement during the SSC of the March 17, 2015 storm. The ground magnetometer at Poker Flat was used to identify the PI and MI phases. During the transition from the PI phase to the MI phase, PFISR observed lifting of the F-region ionosphere, large and transient field-aligned ion upflow, prompt but short-lived ion temperature increase. During the MI phase, PFISR observed F-region density decrease and persistent electron temperature increase in the wake region of the ionospheric flow vortices. The TEC calculated from PFISR density measurement shows a > 7 TECU decrease within a couple of minutes. A global BATSRUS MHD simulation has been

conducted for this event to put localized PFISR observations into a global context. The simulation reveals the distribution of large-scale FACs during the PI and MI phases and their evolution and propagation through the polar cap. The simulated H-component magnetic perturbations at virtual magnetometers placed in the simulation show satisfactory agreement with the Poker Flat magnetometer observations. Based on the simulation results, we demonstrate that the characteristic variations of the ionospheric plasma observed by PFISR are indeed produced by the passage of SC-related current systems.

Combining the observations and numerical simulations together, this case study suggests that transient field-aligned ion upflow and F-region ionosphere lifting due to large vertical flows can be generated due to the SC-related FACs and ionospheric convection flows, providing a plausible explanation for why ion upflow and outflow fluxes increase after the solar wind dynamic pressure increases. Such ionospheric plasma responses should be expected to occur in regions to which the SC-related FACs propagate, and thus may have a global impact, which will be a target of future research. In addition, these observations, for the first time, provide a comprehensive observational confirmation of previous ionospheric simulations on the effects of propagating ionospheric vortices and FAC pairs. Moreover, a deeper understanding of the ionospheric plasma response to SC

and the related FAC system and convection changes will advance our capabilities of forecasting the ionosphere TEC and coherent radar coverage.

Acknowledgements

The research at University of Michigan is supported by NSF AGS 1342968 and NASA NNX14AF31G. We acknowledge use of NASA/GSFC's Space Physics Data Facility's OMNIWeb (or CDAWeb https://cdaweb.sci.gsfc.nasa.gov/index.html/) service, and the OMNI data and Sym-H index. The 1-sec Poker Flat magnetometer data were obtained from the Geophysical Institute, UAF 2016 (https://www.asf.alaska.edu/magnetometer/download/) and the 1-min Poker Flat magnetometer data were obtained from the SuperMag website (http://supermag.jhuapl.edu/). SWMF simulations are performed using the NSF Yellowstone supercomputing facility and will be available by request (shashaz@umich.edu).

References

Araki, T. (1977), Global structure of geomagnetic sudden commencements, *Planetary and Space Science*, *25*(4), 373–384, doi:10.1016/0032-0633(77)90053-8.

Araki, T. (1994) A Physical Model of the Geomagnetic Sudden Commencement, in Solar Wind Sources of Magnetospheric Ultra-Low-Frequency Waves (eds M. J. Engebretson, K. Takahashi and M. Scholer), American Geophysical Union, Washington, D. C.. doi: 10.1029/GM081p0183.

Araki, T. (2013), A Physical Model of the Geomagnetic Sudden Commencement, in *Geophysical Monograph Series*, edited by M. J. Engebretson, K. Takahashi, and M. Scholer, pp. 183–200, American Geophysical Union, Washington, D. C.

Buzulukova, N., M.-C. Fok, J. Goldstein, P. Valek, D. J. McComas, and P. C. Brandt (2010), Ring current dynamics in moderate and strong storms: Comparative analysis of TWINS and IMAGE/HENA data with the Comprehensive Ring Current Model: STRONG STORM VERSUS MODERATE STORM, *Journal of Geophysical Research: Space Physics*, *115*(A12), n/a-n/a, doi:10.1029/2010JA015292.

Charles R. Chappell (2015), The Role of the Ionosphere in Providing Plasma to the Terrestrial Magnetosphere—An Historical Overview, *Space Science Reviews*, *192*(1–4), 5–25, doi:10.1007/s11214-015-0168-5.

Chi, P. J., D.-H. Lee, and C. T. Russell (2006), Tamao travel time of sudden impulses and its relationship to ionospheric convection vortices, *Journal of Geophysical Research*, *111*(A8), doi:10.1029/2005JA011578.

Collis, P. N., and I. Häggström (1991), High-latitude ionospheric response to a geomagnetic sudden commencement, *Journal of Atmospheric and Terrestrial Physics*, *53*(3–4), 241–248, doi:10.1016/0021-9169(91)90108-J.

Curto, J. J., T. Araki, and L. F. Alberca (2007), Evolution of the concept of Sudden Storm Commencements and their operative identification, *Earth, Planets and Space*, *59*(11), i–xii, doi:10.1186/BF03352059.

Doupnik, J. R., A. Brekke, and P. M. Banks (1977), Incoherent scatter radar observations during three sudden commencements and a Pc 5 event on August 4, 1972, *Journal of Geophysical Research*, *82*(4), 499–514, doi:10.1029/JA082i004p00499.

Fok, M.-C., R. A. Wolf, R. W. Spiro, and T. E. Moore (2001), Comprehensive computational model of Earth's ring current, *Journal of Geophysical Research: Space Physics*, *106*(A5), 8417–8424, doi:10.1029/2000JA000235.

Foster, J. C. et al. (2005), Multiradar observations of the polar tongue of ionization, *Journal of Geophysical Research: Space Physics*, *110*(A9), doi:10.1029/2004JA010928.

Friis-Christensen, E., M. A. McHenry, C. R. Clauer, and S. Vennerstrøm (1988), Ionospheric traveling convection vortices observed near the polar cleft: A triggered response to sudden changes in the solar wind, *Geophysical Research Letters*, *15*(3), 253–256, doi:10.1029/GL015i003p00253.

Fujita, S. (2003a), A numerical simulation of the geomagnetic sudden commencement: 1. Generation of the field-aligned current associated with the preliminary impulse, *Journal of Geophysical Research*, *108*(A12), doi:10.1029/2002JA009407.

Fujita, S. (2003b), A numerical simulation of the geomagnetic sudden commencement: 2. Plasma processes in the main impulse, *Journal of Geophysical Research*, *108*(A12), doi:10.1029/2002JA009763.

Fujita, S., T. Tanaka, and T. Motoba (2005), A numerical simulation of the geomagnetic sudden commencement: 3. A sudden commencement in the magnetosphere-ionosphere compound system, *Journal of Geophysical Research*, *110*(A11), doi:10.1029/2005JA011055.

Fukushima, N. (n.d.), Generalized theorem for no ground magnetic effect of vertical currents connected with Pedersen currents in the uniform-conductivity ionosphere,

Gillies, D. M., J.-P. St.-Maurice, K. A. McWilliams, and S. Milan (2012), Global-scale observations of ionospheric convection variation in response to sudden increases in the solar wind dynamic pressure, *Journal of Geophysical Research: Space Physics*, *117*(A4), n/a-n/a, doi:10.1029/2011JA017255.

Glassmeier, K.-H., M. Hönisch, and J. Untiedt (1989), Ground-based and satellite observations of traveling magnetospheric convection twin vortices, *Journal of Geophysical Research*, *94*(A3), 2520, doi:10.1029/JA094iA03p02520.

Glocer, A., M. Fok, X. Meng, G. Toth, N. Buzulukova, S. Chen, and K. Lin (2013), CRCM + BATS-R-US two-way coupling, *Journal of Geophysical Research: Space Physics*, *118*(4), 1635–1650, doi:10.1002/jgra.50221.

Heinselman, C. J., and M. J. Nicolls (2008), A Bayesian approach to electric field and *E* -region neutral wind estimation with the Poker Flat Advanced Modular Incoherent Scatter Radar, *Radio Science*, *43*(5), n/a-n/a, doi:10.1029/2007RS003805.

Kane, T. A., and R. A. Makarevich (2010), HF radar observations of the *F* region ionospheric plasma response to Storm Sudden Commencements, *Journal of Geophysical Research: Space Physics*, *115*(A7), n/a-n/a, doi:10.1029/2009JA014974.

Kataoka, R., H. Fukunishi, K. Hosokawa, H. Fujiwara, A. S. Yukimatu, N. Sato, and Y.-K. Tung (2003), Transient production of F-region irregularities associated with TCV passage, *Annales Geophysicae*, *21*(7), 1531–1541, doi:10.5194/angeo-21-1531-2003.

Kikuchi, T., S. Tsunomura, K. Hashimoto, and K. Nozaki (2001), Field-aligned current effects on midlatitude geomagnetic sudden commencements, *Journal of Geophysical Research: Space Physics*, *106*(A8), 15555–15565, doi:10.1029/2001JA900030.

Kivelson, M. G., and D. J. Southwood (1991), Ionospheric traveling vortex generation by solar wind buffeting of the magnetosphere, *Journal of Geophysical Research: Space Physics*, *96*(A2), 1661–1667, doi:10.1029/90JA01805.

Kubota, Y., R. Kataoka, M. Den, T. Tanaka, T. Nagatsuma, and S. Fujita (2015), Global MHD simulation of magnetospheric response of preliminary impulse to large and

sudden enhancement of the solar wind dynamic pressure, *Earth, Planets and Space*, *67*(1), doi:10.1186/s40623-015-0270-7.

Kurazhkovskaya, N. A., and B. I. Klain (2016), Geomagnetic (MIE) and storm sudden commencement (SSC) impulses in a high-latitude magnetosphere, *Geomagnetism and Aeronomy*, *56*(1), 30–41, doi:10.1134/S0016793216010102.

Lanzerotti, L. J., R. M. Konik, A. Wolfe, D. Venkatesan, and C. G. Maclennan (1991), Cusp latitude magnetic impulse events: 1. Occurrence statistics, *Journal of Geophysical Research: Space Physics*, *96*(A8), 14009–14022, doi:10.1029/91JA00567.

Lotko, W. (2007), The magnetosphere–ionosphere system from the perspective of plasma circulation: A tutorial, *Journal of Atmospheric and Solar-Terrestrial Physics*, *69*(3), 191–211, doi:10.1016/j.jastp.2006.08.011.

Lühr, H., W. Blawert, and H. Todd (1993), The ionospheric plasma flow and current patterns of travelling convection vortices: a case study, *Journal of Atmospheric and Terrestrial Physics*, *55*(14), 1717–1727, doi:10.1016/0021-9169(93)90140-T.

Moretto, T., E. Friis-Christensen, H. Lühr, and E. Zesta (1997), Global perspective of ionospheric traveling convection vortices: Case studies of two Geospace Environmental Modeling events, *Journal of Geophysical Research: Space Physics*, *102*(A6), 11597–11610, doi:10.1029/97JA00324.

Murr, D. L. (2002), Conjugate observations of traveling convection vortices: The field-aligned current system, *Journal of Geophysical Research*, *107*(A10), doi:10.1029/2002JA009456.

Murr, D. L., and W. J. Hughes (2003), Solar wind drivers of Traveling Convection Vortices, *Geophysical Research Letters*, *30*(7), doi:10.1029/2002GL015498.

Nilsson, H. et al. (2008), Transients in oxygen outflow above the polar cap as observed by the Cluster spacecraft, *Annales Geophysicae*, *26*(11), 3365–3373, doi:10.5194/angeo-26-3365-2008.

Nishida, A., and J. A. Jacobs (1962), World-wide changes in the geomagnetic field, *Journal of Geophysical Research*, *67*(2), 525–540, doi:10.1029/JZ067i002p00525.

Ogawa, Y., S. C. Buchert, R. Fujii, S. Nozawa, and A. P. van Eyken (2009), Characteristics of ion upflow and downflow observed with the European Incoherent Scatter Svalbard radar, *Journal of Geophysical Research: Space Physics*, *114*(A5), n/a-n/a, doi:10.1029/2008JA013817.

Ogawa, Y., R. Fujii, S. C. Buchert, S. Nozawa, S. Watanabe, *and* A. P. van Eyken *(*2000*),* Simultaneous EISCAT Svalbard and VHF radar observations of ion upflows at different aspect angles, Geophys. Res. Lett., 27*(*1*),* 81–84, *doi:*10.1029/1999GL010665.

Richards, P. G., and D. Voglozin (2011), Reexamination of ionospheric photochemistry, *Journal of Geophysical Research: Space Physics*, *116*(A8), n/a-n/a, doi:10.1029/2011JA016613.

Ridley, A. J., and M. W. Liemohn (2002), A model-derived storm time asymmetric ring current driven electric field description, *Journal of Geophysical Research: Space Physics*, *107*(A8), SMP 2-1-SMP 2-12, doi:10.1029/2001JA000051.

Ridley, A. J., T. I. Gombosi, and D. L. DeZeeuw (2004), Ionospheric control of the magnetosphere: conductance, *Annales Geophysicae*, *22*(2), 567–584, doi:10.5194/angeo-22-567-2004.

Samsonov, A. A., D. G. Sibeck, and Y. Yu (2010), Transient changes in magnetospheric-ionospheric currents caused by the passage of an interplanetary shock: Northward interplanetary magnetic field case, *Journal of Geophysical Research: Space Physics*, *115*(A5), n/a-n/a, doi:10.1029/2009JA014751.

Schunk, R., *and* A. Nagy *(*2009*),* Ionospheres: Physics, Plasma Physics, and Chemistry, *Cambridge Univ. Press,* Cambridge.

Schunk, R. W., L. Zhu, and J. J. Sojka (1994), Ionospheric response to traveling convection twin vortices, *Geophysical Research Letters*, *21*(17), 1759–1762, doi:10.1029/94GL01059.

Semeter, J., C. J. Heinselman, J. P. Thayer, R. A. Doe, and H. U. Frey (2003), Ion upflow enhanced by drifting *F* -region plasma structure along the nightside polar cap boundary, *Geophysical Research Letters*, *30*(22), doi:10.1029/2003GL017747.

Shi, Q. Q. et al. (2014), Solar wind pressure pulse-driven magnetospheric vortices and their global consequences, *Journal of Geophysical Research: Space Physics*, *119*(6), 4274–4280, doi:10.1002/2013JA019551.

Shinbori, A., Y. Tsuji, T. Kikuchi, T. Araki, A. Ikeda, T. Uozumi, D. Baishev, B. M. Shevtsov, T. Nagatsuma, and K. Yumoto (2012), Magnetic local time and latitude dependence of amplitude of the main impulse (MI) of geomagnetic sudden commencements and its seasonal variation, *Journal of Geophysical Research: Space Physics*, *117*(A8), n/a-n/a, doi:10.1029/2012JA018006.

Sibeck, D. G., and G. I. Korotova (1996), Occurrence patterns for transient magnetic field signatures at high latitudes, *Journal of Geophysical Research: Space Physics*, *101*(A6), 13413–13428, doi:10.1029/96JA00187.

Sibeck, D. G., N. B. Trivedi, E. Zesta, R. B. Decker, H. J. Singer, A. Szabo, H. Tachihara, and J. Watermann (2003), Pressure-pulse interaction with the magnetosphere and ionosphere, *Journal of Geophysical Research: Space Physics*, *108*(A2), doi:10.1029/2002JA009675.

Slinker, S. P., J. A. Fedder, W. J. Hughes, and J. G. Lyon (1999), Response of the ionosphere to a density pulse in the solar wind: Simulation of traveling convection

vortices, *Geophysical Research Letters*, *26*(23), 3549–3552, doi:10.1029/1999GL010688.

Strangeway, R. J. (2005), Factors controlling ionospheric outflows as observed at intermediate altitudes, *Journal of Geophysical Research*, *110*(A3), doi:10.1029/2004JA010829.

Sun, T. R., C. Wang, J. J. Zhang, V. A. Pilipenko, Y. Wang, and J. Y. Wang (2015), The chain response of the magnetospheric and ground magnetic field to interplanetary shocks, *Journal of Geophysical Research: Space Physics*, *120*(1), 157–165, doi:10.1002/2014JA020754.

Tian, A. M., X. C. Shen, Q. Q. Shi, B. B. Tang, M. Nowada, Q. G. Zong, and S. Y. Fu (2016), Dayside magnetospheric and ionospheric responses to solar wind pressure increase: Multispacecraft and ground observations, *Journal of Geophysical Research: Space Physics*, doi:10.1002/2016JA022459.

Tóth, G. et al. (2012), Adaptive numerical algorithms in space weather modeling, *Journal of Computational Physics*, *231*(3), 870–903, doi:10.1016/j.jcp.2011.02.006.

Winser, K. J., M. Lockwood, G. O. L. Jones, *and* K. Suvanto *(*1989*),* Observations of nonthermal plasmas at different aspect angles, J. Geophys. Res., 94*(*A2*),* 1439–1449*, doi:*10.1029/JA094iA02p01439.

Yau, A. W., T. Abe, and W. K. Peterson (2007), The polar wind: Recent observations, *Journal of Atmospheric and Solar-Terrestrial Physics*, *69*(16), 1936–1983, doi:10.1016/j.jastp.2007.08.010.

Yu, Y.-Q., and A. J. Ridley (2011), Understanding the response of the ionosphere-magnetosphere system to sudden solar wind density increases, *Journal of Geophysical Research: Space Physics*, *116*(A4), n/a-n/a, doi:10.1029/2010JA015871.

Yuan, Z.-G., X.-H. Deng, and J.-F. Wang (2008), DMSP/GPS observations of intense ion upflow in the midnight polar ionosphere associated with the SED plume during a super geomagnetic storm, *Geophysical Research Letters*, *35*(19), doi:10.1029/2008GL035462.

Zesta, E. (2002), A statistical study of traveling convection vortices using the Magnetometer Array for Cusp and Cleft Studies, *Journal of Geophysical Research*, *107*(A10), doi:10.1029/1999JA000386.

Zesta, E., W. J. Hughes, M. J. Engebretson, T. J. Hughes, A. J. Lazarus, and K. I. Paularena (1999), The November 9, 1993, traveling convection vortex event: A case study, *Journal of Geophysical Research: Space Physics*, *104*(A12), 28041–28058, doi:10.1029/1999JA900306.

Zettergren, M., J. Semeter, C. Heinselman, and M. Diaz (2011), Incoherent scatter radar estimation of *F* region ionospheric composition during frictional heating events,

Journal of Geophysical Research: Space Physics, *116*(A1), n/a-n/a, doi:10.1029/2010JA016035.

Zhang, S.-R., P. J. Erickson, Y. Zhang, W. Wang, C. Huang, A. J. Coster, J. M. Holt, J. F. Foster, M. Sulzer, and R. Kerr (2017), Observations of ion-neutral coupling associated with strong electrodynamic disturbances during the 2015 St. Patrick's Day storm, *Journal of Geophysical Research: Space Physics*, *122*(1), 1314–1337, doi:10.1002/2016JA023307.

Zou, S., M. B. Moldwin, M. J. Nicolls, A. J. Ridley, A. J. Coster, E. Yizengaw, L. R. Lyons, and E. F. Donovan (2013), Electrodynamics of the high-latitude trough: Its relationship with convection flows and field-aligned currents, *Journal of Geophysical Research: Space Physics*, *118*(5), 2565–2572, doi:10.1002/jgra.50120.

Zou, S., M. B. Moldwin, A. J. Ridley, M. J. Nicolls, A. J. Coster, E. G. Thomas, and J. M. Ruohoniemi (2014), On the generation/decay of the storm-enhanced density plumes: Role of the convection flow and field-aligned ion flow, *Journal of Geophysical Research: Space Physics*, *119*(10), 8543–8559, doi:10.1002/2014JA020408.

Zou, S., A. Ridley, X. Jia, E. Boyd, M. Nicolls, A. Coster, E. Thomas, and J. M. Ruohoniemi (2017), PFISR observation of intense ion upflow fluxes associated

with an SED during the 1 June 2013 geomagnetic storm, *Journal of Geophysical Research: Space Physics*, doi:10.1002/2016JA023697.

Figure Captions

Figure 1: From top to bottom, IMF B_y, B_z components in the GSM coordinates, solar wind speed, proton number density, solar wind dynamic pressure and the *Sym-H* index are shown for 03-07 UT on March 17, 2015. The vertical dashed line indicates the beginning of the storm sudden commencement (SSC) signature in the Sym-H index at ~0445 UT.

Figure 2: The top panel shows the 1-sec magnetic perturbation in the H component measured by the magnetometer at Poker Flat. The average value in the first 10 minutes has been subtracted from the measured field. The vertical dashed line indicates the beginning of the preliminary impulse (PI) phase at ~0445 UT. PFISR measurements from 0430 to 0500 UT on March 17, 2015 are shown in Figure 2b-2g. From top to bottom, figure 2b-2g show (b) *ExB* convection flow direction, (c) flow speed, (d) flow vectors, (e) calculated vertical plasma flows, (f) contribution of the vertical flows from the ExB convection flows (red) and the antiparallel flow measured along the magnetic field line (blue), (g) the raw electron densities with no correction for Te/Ti or Debye length effects measured by beam 1, respectively. Beam 1 points vertically in the geographic

coordinates.

Figure 3: Vertical profiles of (a) electron density, (b) line-of-sight velocity, (c) ion temperature, and (d) electron temperature measured by the PFISR vertical beam 1. Grey curves show the measurements prior to the SC-related FAC passage; Blue curves show the measurements during the passage of SC-related FAC; Green and red curves show the measurements after the SC-related FAC. Error bars indicate the measurement uncertainties. (e) field-aligned line-of-sight velocities measured by beam 2, i.e., the field-aligned beam, at 0447:22-0448:32 UT (red) and 0448:32-0449:42 UT (blue) are shown. Only data points with measurement uncertainty smaller than the magnitude of measurement itself are plotted. Field-aligned ion upflow event can be identified at both time cadences.

Figure 4: (a) Comparison between the simulated magnetic perturbations in the H component and the observations at Poker Flat. 1-min time resolution data are used here. (b-c) 2D distribution of simulated magnetic perturbations in the H component at the dip of the PI phase and the peak of the MI phase in the northern hemisphere. (d-e) 2D distribution of simulated field-aligned currents (FACs) and convection equipotentials in the northern hemisphere. The open-closed field line boundary is shown as purple lines.

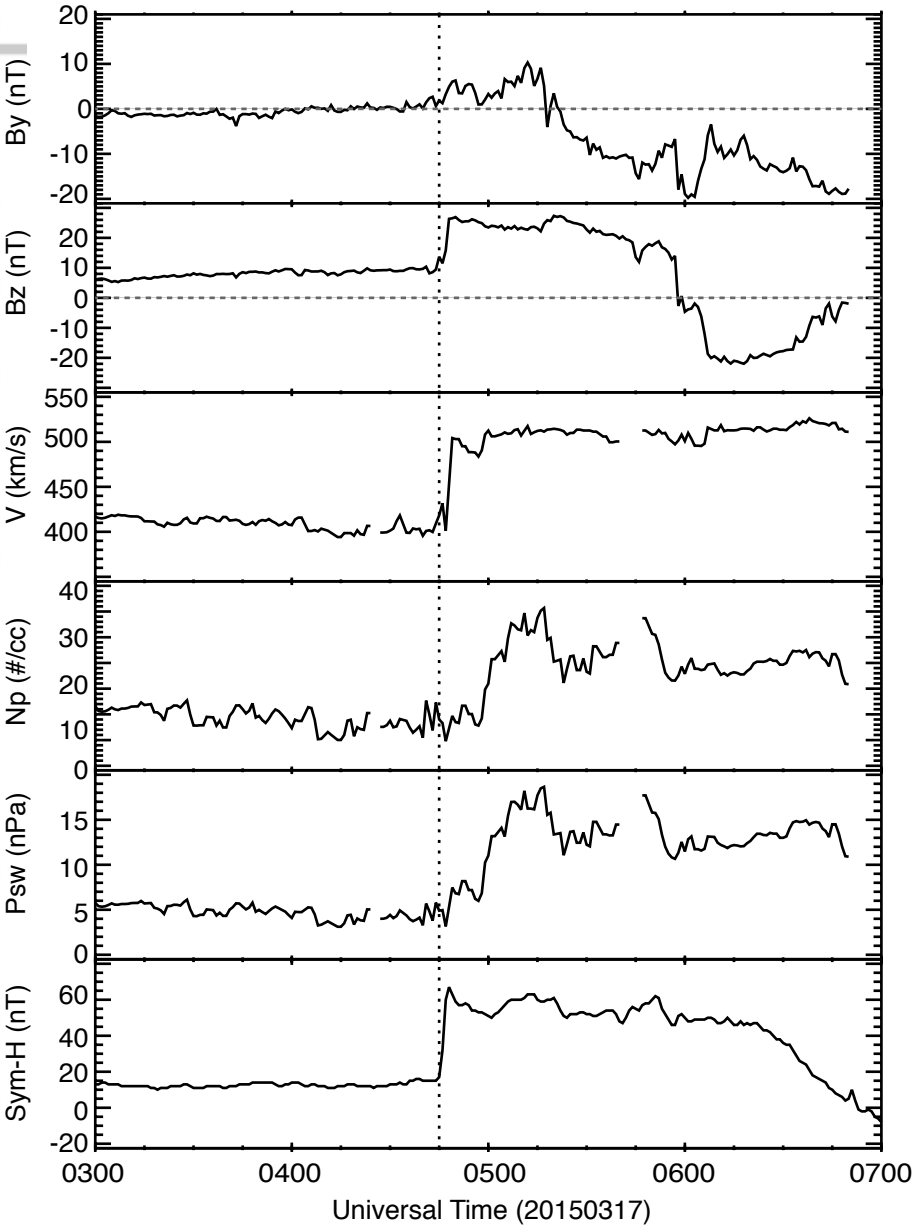

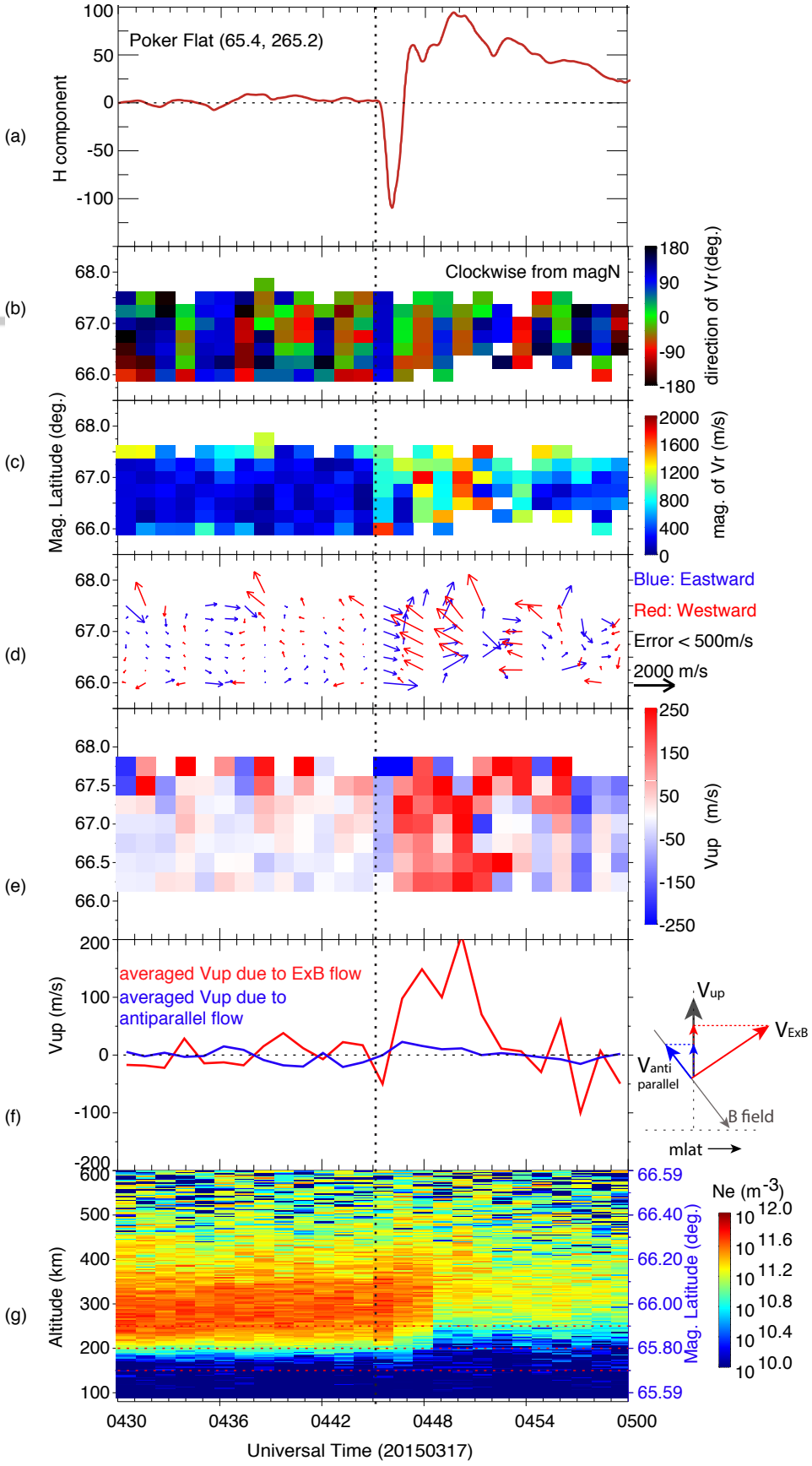

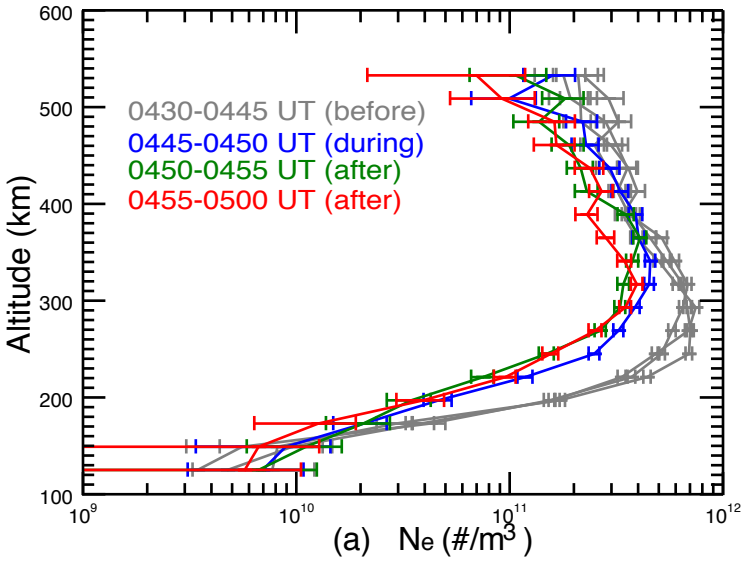

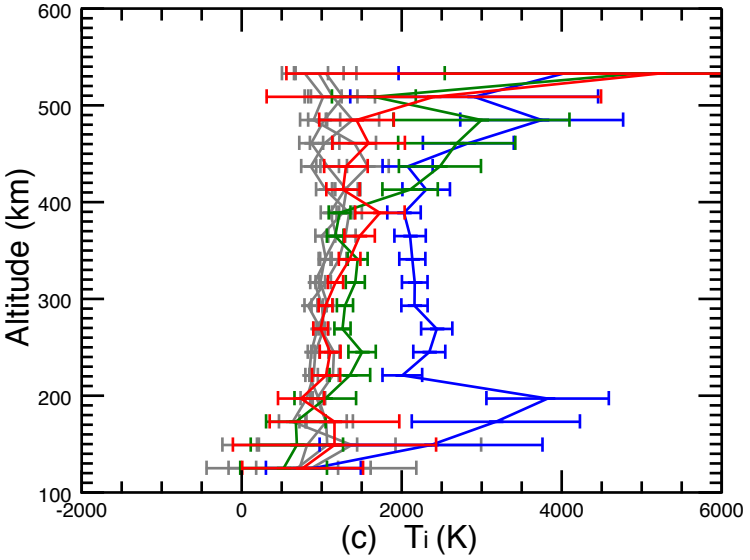

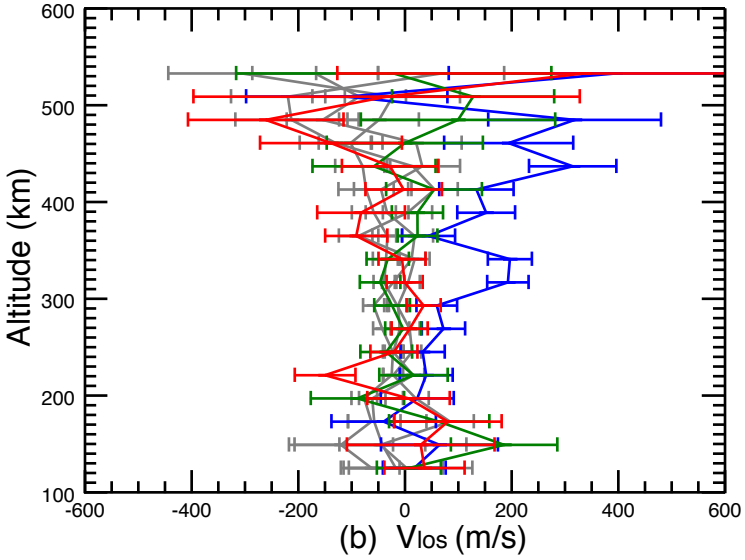

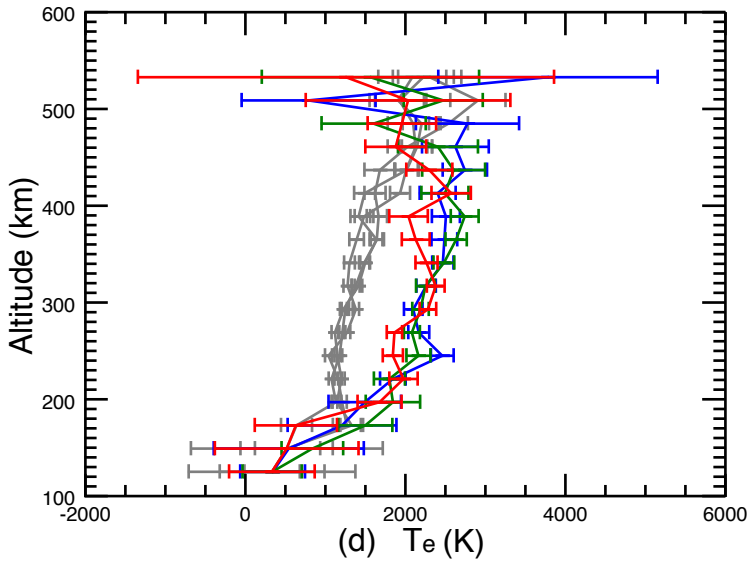

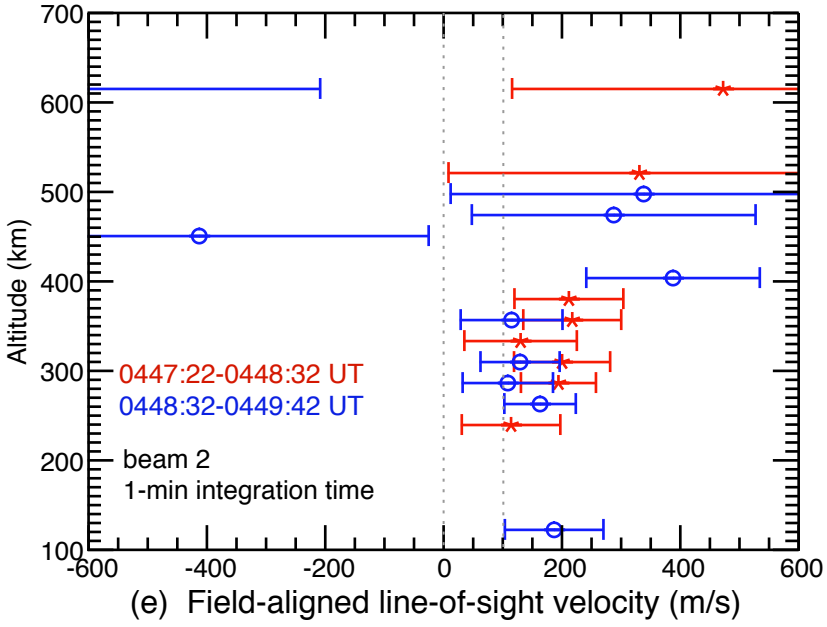

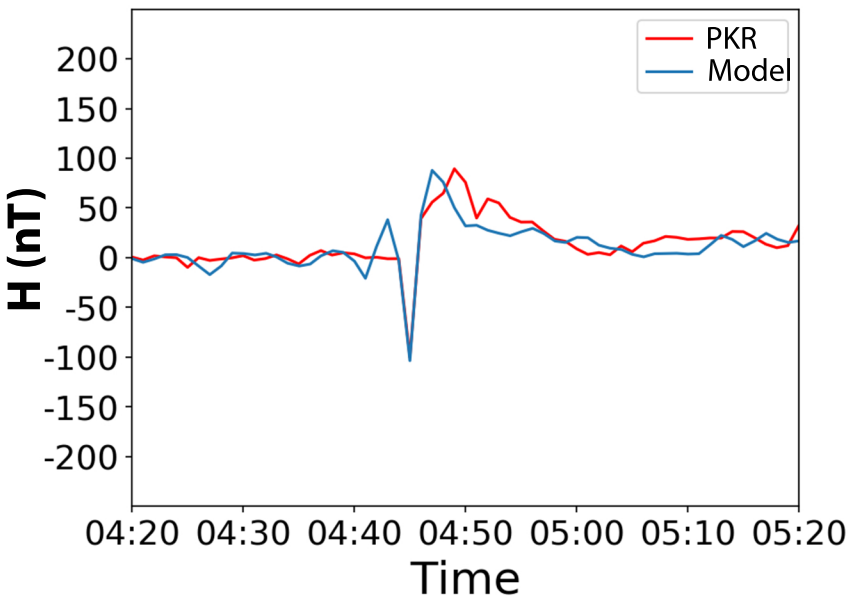

(a)

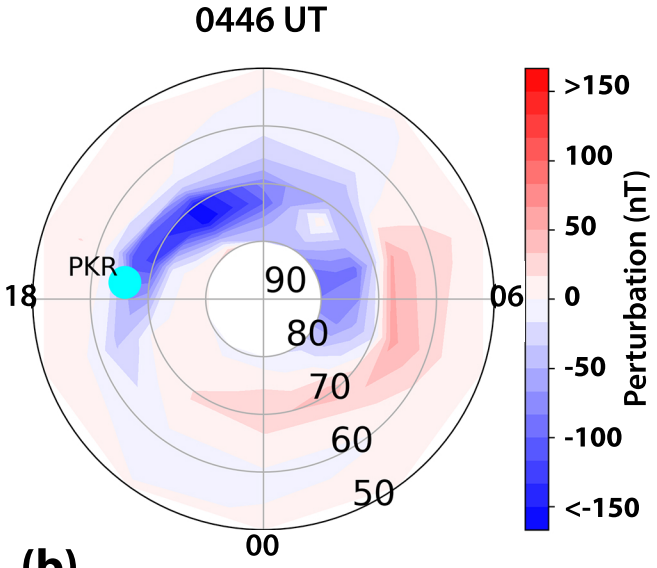

(b)

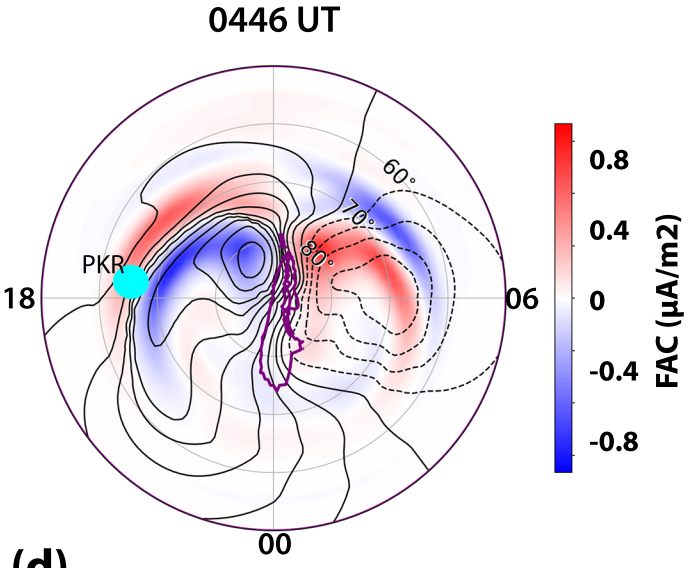

(d)

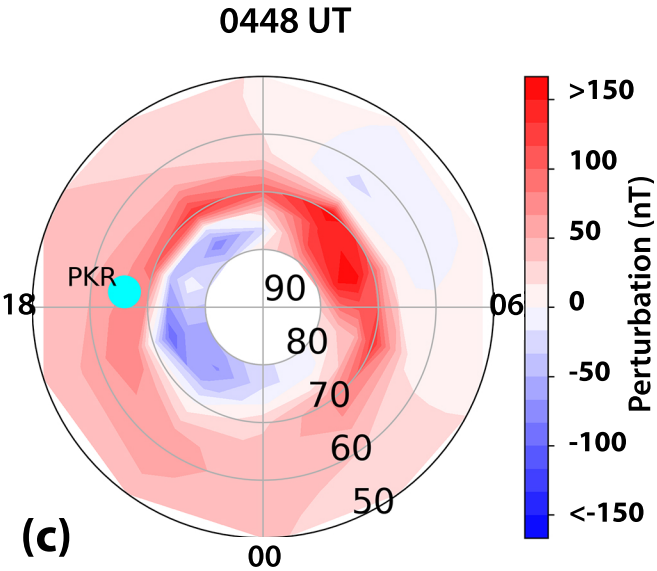

(c)

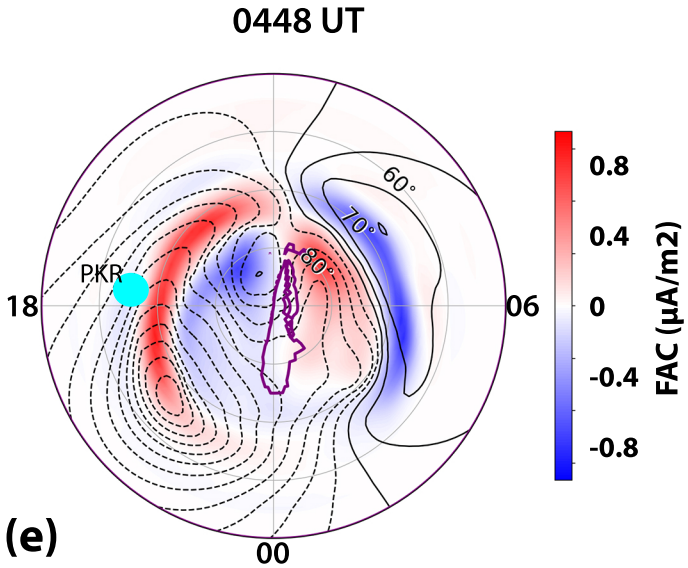

(e)